Rapid Communications

Shear-induced migration and orientation of rigid fibers in an oscillatory pipe flow

Scott Strednak,[1,2] Saif Shaikh,[1,2] Jason E. Butler,[2] and Élisabeth Guazzelli[1]
[1]*Aix-Marseille Univ, CNRS, IUSTI, Marseille, France*
[2]*Department of Chemical Engineering, University of Florida, Gainesville, Florida 32611, USA*

(Received 8 June 2018; published 10 September 2018)

The spatial and orientation distributions of fibers in suspension were measured during oscillatory flow within a circular pipe. The fibers were rigid and non-colloidal, and two aspect ratios (length L to diameter d ratios) of $L/d = 11$ and 23 were tested; the suspending fluid was viscous, Newtonian, and density matched to the particles. As with shear-induced migration of spheres in parabolic flows, fibers in the concentrated suspensions migrated toward the center of the pipe. The migration was similar for the fibers, irrespective of the aspect ratio, at the same dimensionless number density n_0L^2d (n_0 is the number of fibers per unit volume of the bulk suspension), rather than at the same volume fraction. The extent of migration was maximum at $n_0L^2d = 0.84$ for both aspect ratios. The orientation distribution of the fibers was spatially dependent. Fibers near the center of the channel aligned closely with the flow direction, while fibers near the pipe wall had an enhanced probability of aligning in the vorticity direction.

DOI: 10.1103/PhysRevFluids.3.091301

Adding even a small volume fraction of fibers to a fluid can impact its rheological properties substantially [1], and such additives are often used to improve the performance of materials such as fiber reinforced composites and concrete [2]. In these applications, the spatial and orientation distribution of the particles strongly influences the rheology, and even the final properties. While orientation distributions have been measured in steady and oscillatory shearing flows [3–5], few experiments have investigated the spatial distribution of rigid fibers.

For spherical particles suspended at large concentration in unidirectional flows, shear-induced migration from regions of high to low shear rates has been observed [6–14]. This transverse migration has been shown to be driven by spatial variations in the normal stresses of the particle phase [15,16]. However, these normal stresses are qualitatively different for suspensions of fibers and spheres [17], and whether migration is similar for suspensions of different particle shapes is still relatively unknown. The one experimental result available is qualitatively consistent with that found for spheres [18]. This experiment used non-Brownian, neutrally buoyant fibers suspended in a viscous fluid undergoing shear in a wide-gap Couette cell. The fibers migrated toward the outer wall of the Couette cell, and the steady concentration profile was reported to be independent of the aspect ratio (fiber length to diameter) over a range from 2 to 18.4 at identical volume fractions.

The objective of this Rapid Communication is to determine whether migration occurs for rigid fibers in a pressure-driven flow, and, if so, whether migration is toward the center, as expected for spheres, or not. To our knowledge, no measurements have been made for pressure-driven flows, though the results of some calculations have been reported [19,20]. The present experiments study two aspect ratios and bulk concentrations spanning a factor of 3. The imposed flow in the pipe is oscillatory, rather than steady; studies of spheres in oscillatory pressure-driven flows [21,22] indicate that the migration is similar, at least qualitatively, to the migration in steady flows as long as the amplitude of displacement is much larger than the pipe radius. The fibers are shown

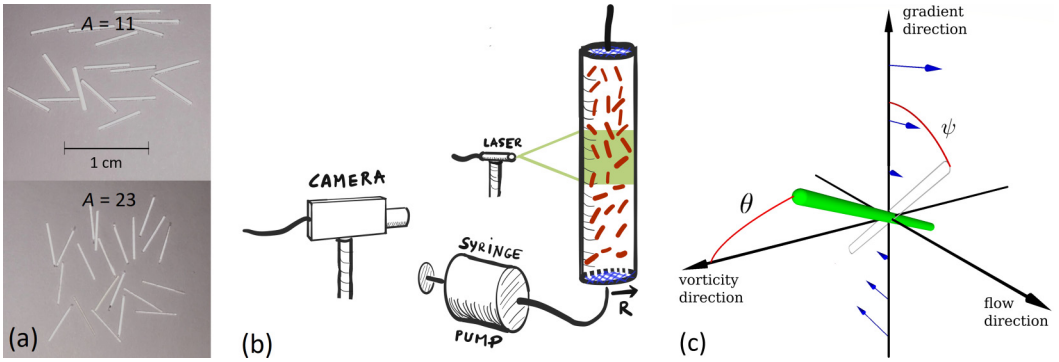

FIG. 1. (a) Photographs of the PMMA fibers of aspect ratio $A = 11 \pm 2$ and 23 ± 2. (b) Sketch of the experimental apparatus. Its major features include the syringe pump, which oscillates flow of the suspension in the pipe of radius R, and the laser sheet, which fluoresces the suspending fluid and enables imaging with a digital camera. (c) The fiber orientation is defined by the angle θ between its major axis and the vorticity direction and the angle ψ that the projection of the fiber makes onto the flow-gradient plane with the gradient direction.

to concentrate along the centerline, and our measurements indicate that the migration depends upon the bulk concentration ($n_0 L^2 d$), rather than the volume fraction ($\propto n_0 L d^2$). These results, as well as information for the orientation distribution, are given after the description of the measurement techniques.

Two batches of fibers were manufactured from fiber optic filaments with poly(methyl methacrylate) (PMMA) cores of diameter $d = 0.46 \pm 0.06$ and 0.23 ± 0.02 mm. The filaments were soaked in dimethyl sulfoxide, mechanically wiped to remove the outer fluorocarbon coating, and then cut into segments of length $L = 5.2 \pm 0.2$ mm to produce fibers with aspect ratios of $A = L/d = 11 \pm 2$ and 23 ± 2. The fibers [see Fig. 1(a)] were suspended in a mixture of Triton X-100 (73% by mass), distilled water (11%), and zinc chloride (16%). Fluorescent dye (Rhodamine 6G) was added to the mixture at a concentration of 9×10^{-7} g/mL. This fluid was Newtonian, with a viscosity of 30 P at 25 °C, and the density and refractive index matched that of the fibers. Suspensions were prepared at bulk concentrations of $n_0 L^2 d$ between 0.42 and 3.00, where n_0 was the number of rods per unit volume. Note that the dimensionless number density, $n_0 L^2 d$, is related to the bulk volume fraction, ϕ_0, by the relation $n_0 L^2 d = 4A\phi_0/\pi$.

The experimental setup, similar to that used to study shear-induced migration of spheres [22], is shown in Fig. 1(b). The suspension was loaded into an acrylic pipe of length 46.8 cm and radius $R = 0.825$ cm. The pipe was oriented vertically, and a mesh screen was placed at the top and bottom ends to maintain a constant particle concentration within the testing section. The pipe was connected to a syringe pump that cyclically displaced the fluid at a fixed amplitude, where the rate of volumetric fluid displacement, as a function of time t, was $(\gamma_0 R)(\pi R^2)\omega \cos(\omega t)/|\cos(\omega t)|$. The strain amplitude was chosen to be $\gamma_0 = 15$ in all of the experiments in order to minimize possible end effects, while also having a net displacement that was large compared to the pipe radius. The frequency ω used in the experiments gives a Reynolds number less than 10^{-3} and a Péclet number greater than 10^9, meeting the conditions for a Stokes flow of non-Brownian particles. The maximum stress exerted by the flow on the fibers was much smaller than the stress required to buckle a fiber [23]; consequently the fibers were considered rigid.

The acrylic pipe was jacketed by a rectangular plexiglass box filled with suspending fluid that contained no particles or dye. This jacket facilitated imaging the suspension by eliminating optical distortion caused by the curvature of the pipe. A laser sheet of width 250 μm and wavelength 532 nm fluoresced the dyed fluid, but not the particles, in a vertical plane passing through the center of the pipe. A shutter was mounted in front of the laser to prevent photobleaching caused by overexposure

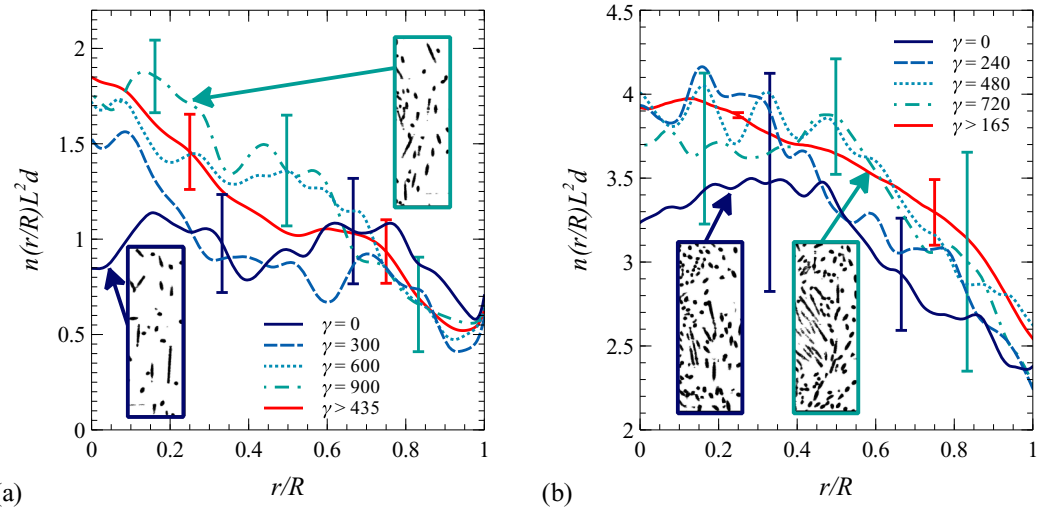

FIG. 2. Concentration, $n(r/R)L^2d$, versus position, r/R, for (a) $n_0L^2d = 0.84$ and (b) $n_0L^2d = 3.00$ at four values of the accumulated strain γ. Results are for $A = 11$ and the error bars represent the standard error computed across multiple experimental runs. Example images from the initial and last oscillations showing the processed results from $r/R = 0$, on the left side of each image, to $r/R = 1$, on the right side of each image. Accompanying Movies 4 and 5 [24] show comparisons between the original and processed images, as well as $n(r/R)L^2d$, for both bulk concentrations at every oscillation. The solid red line in each plot shows the concentration versus position averaged over accumulated strains that correspond to steady state.

of the fluid and a high-resolution camera recorded images of the illuminated plane. The shutter and camera were actuated by the microcontroller used to operate the syringe pump.

The suspension was added to the inner circular pipe, gently mixed, and allowed to stand to enable any trapped air to escape before starting each experiment. Forty images were taken with 1-s intervals at the beginning of each cycle. This procedure was repeated at least three times for every set of conditions (bulk concentration and aspect ratio). Movies 1–3 [24] in the Supplemental Material (SM) show many example images.

The experimental images were processed using classical image analysis (adaptive contrast enhancement, adaptive thresholding, and removal of objects smaller than a defined size); see Fig. 2(a) for example results. Note that only the half of the image closest to the laser was processed due to degradation of the image quality in the other half. Quantitative data were extracted from the processed images, where the dark pixels represent the fibers. The areal fraction of dark pixels in each vertical row of pixels was calculated and converted to a volume fraction $\phi(r)$ by assuming that the distribution is independent of the angular position in the pipe. The volume fraction $\phi(r)$ was multiplied by $4A/\pi$ to give the position-dependent concentration $n(r)L^2d$. To test the image analysis, $n(r)$ was integrated across the pipe radius to give n_b; n_b was calculated to be within 10% of the bulk value n_0 for all cases except $n_0L^2d = 0.42$, which gives a difference of 28%.

Information about the orientation distribution was also extracted from the processed images. The angles θ and ψ [see Fig. 1(c)] can be calculated from the observable length and angle in the plane of the laser sheet, respectively, for cases where the laser sheet intersects the center of mass of a fiber. In all other cases, the velocity gradient and vorticity directions evaluated at the center of mass of a fiber do not correspond to the velocity gradient and vorticity directions in the plane of the laser sheet since the flow occurs within a cylinder. Consequently, we report the probability distributions of θ' and ψ', the observed angles relative to the gradient and vorticity directions at the point where the fiber intersects the laser sheet rather than at its center. Note that a value of ψ' cannot be determined if $\theta' < 34^\circ$ for $A = 11$ and $\theta' < 24^\circ$ for $A = 23$, so these cases were excluded when calculating the

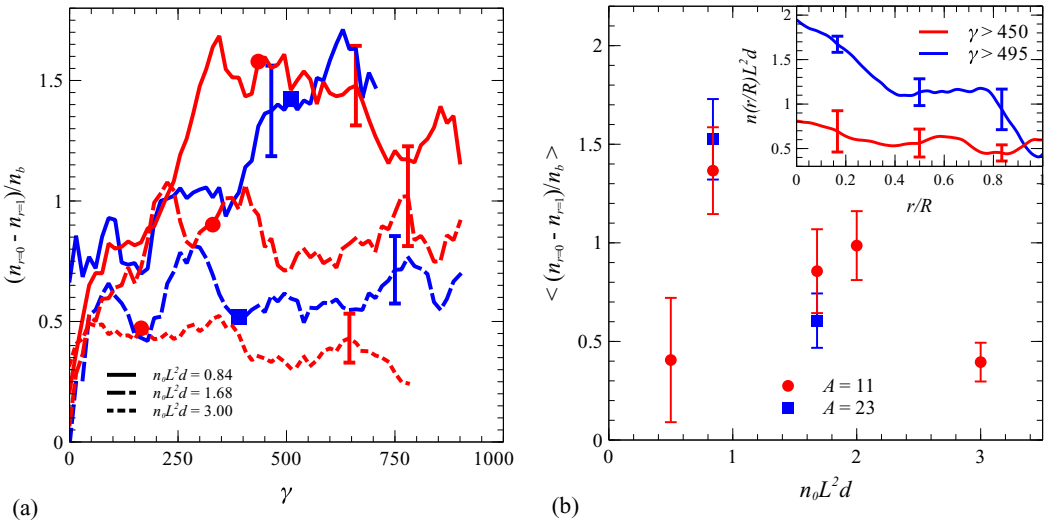

FIG. 3. (a) Extent of migration versus accumulated strain, γ, for $A = 11$ (red) and $A = 23$ (blue) at multiple bulk concentrations. (b) Extent of migration at steady state versus n_0L^2d for $A = 11$ and 23, where the averaging was performed over accumulated strains larger than those marked by the solid circles or squares in (a). The error bars represent the standard deviations computed across multiple experiments. The inset shows the concentration versus position averaged over accumulated strains that corresponds to steady state for $n_0L^2d = 0.42$ and $A = 11$ (red line) and $n_0L^2d = 0.84$ and $A = 23$ (blue line); in both cases, $\phi_0 \approx 0.03$.

probability distribution $P(\psi')$. Also, the length observed in the images can represent multiple values of θ' for fibers closely aligned with the flow direction; hence all instances of $\theta' > 82^\circ$ for $A = 11$ and $\theta' > 85^\circ$ for $A = 23$ were lumped into the same data point (bin) when calculating $P(\theta')$.

Figure 2(a) shows processed images for $n_0L^2d = 0.84$ and $A = 11$ which qualitatively illustrate that the spatial distribution of fibers moves from a roughly uniform one at $\gamma = 0$ to one with particles preferentially located near the center of the pipe ($r/R = 0$) for $\gamma = 900$. This shear-induced migration was quantified by calculating the radially dependent areal fraction of dark pixels from each image and averaging over multiple experimental runs. These areal fractions are plotted in the graphs of Fig. 2(a) after having converted them to local concentrations, $n(r/R)L^2d$. As strain accumulated, the particle concentration increased in the center of the pipe and decreased near the walls, showing evidence of shear-induced migration for suspensions for this set of conditions. Likewise, Fig. 2(b) shows examples of processed images and the spatial distribution of fibers for a larger concentration of $n_0L^2d = 3.00$ at $A = 11$. The initial distribution at $\gamma = 0$ exhibits a difference between the concentrations $n(r/R)$ at the center and wall. Still, some migration of particles toward the center of the pipe was observed as the strain accumulated.

A single metric, the extent of migration, was used to evaluate the rate of migration and to compare the final particle distribution over different aspect ratios and bulk concentrations n_0L^2d. The extent of migration is $(n_{r=0} - n_{r=1})/n_b$, where $n_{r=0}$ is the number density in a region of width $R/16$ at the center of the pipe and $n_{r=1}$ is the number density in a region of width $R/16$ near the wall of the pipe.

Figure 3(a) shows the extent of migration as a function of the accumulated strain for $A = 11$ and 23 for multiple bulk concentrations. The values shown correspond to a moving mean over a strain of 75 that has been averaged over multiple experimental runs. The extent of migration increases with accumulated strain until it reaches a steady value (even though the fluctuations are large), and the more concentrated suspensions attain a steady particle distribution at lower accumulated strains. Figure 3(b) shows the dependence of the extent of migration on bulk concentration at steady state for both $A = 11$ and 23. Irrespective of the aspect ratio, the steady value of the extent of migration

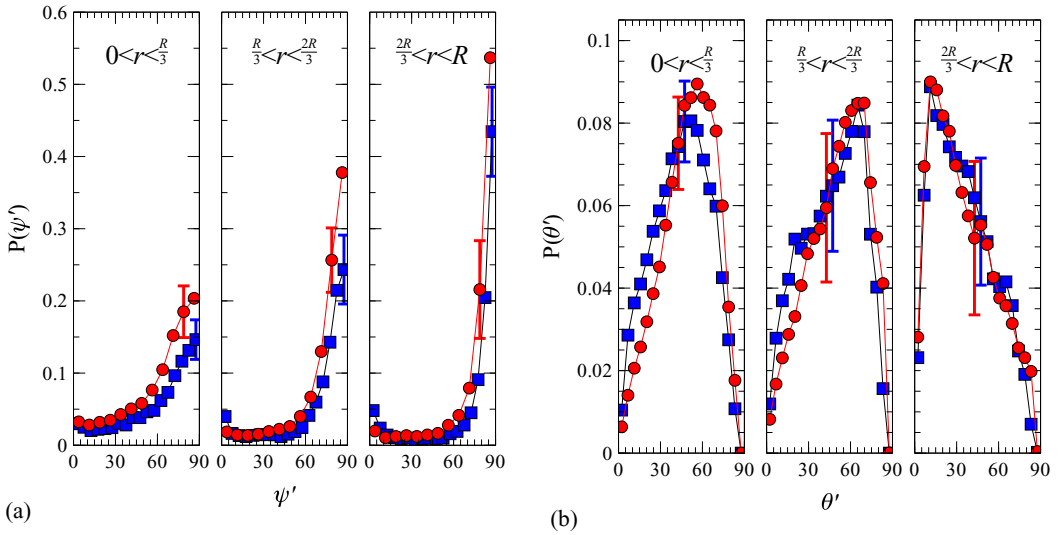

FIG. 4. Probability of finding a particle at (a) an angle ψ' and (b) an angle θ' for the center ($0 < r < R/3$), middle ($R/3 < r < 2R/3$), and near-wall portions ($2R/3 < r < R$) of the pipe. Results are shown for $n_0L^2d = 0.84$ and aspect ratios of $A = 11$ (red circles) and 23 (blue squares).

was found to be the same within the experimental error at the same value of n_0L^2d. Note also that the rates of migration are similar for the two aspect ratios.

Data on the orientation distribution for steady-state conditions are presented in Fig. 4 for $n_0L^2d = 0.84$, the concentration at which the extent of migration was maximum [see Fig. 3(b)]. Probability distributions for both ψ' and θ' are shown in each of three radial bins of equal size, where the integrated distribution has been normalized to 1 in each bin. Differences in the orientations between experiments at $A = 11$ and 23 are small, and are within the measurement errors. A large proportion of fibers have a value of ψ' near 90°, and few near 0°, which is consistent with preferential fiber alignment in the flow, rather than the gradient, direction. This tendency to align with the axial flow is strongest for $2R/3 < r < R$, where the wall constrains the allowable orientations. The wall also impacts the distribution of θ'; as seen in Fig. 4(b), it shifts toward zero as the radial position increases. This implies that the fibers near the wall have an enhanced probability of aligning with the vorticity direction of the flow.

In this work, quantitative measurements of the spatial distribution of rigid fibers in a parabolic flow show that the particles migrate toward the center of the pipe. This is qualitatively consistent with observations of shear-induced migration of spheres, where particles concentrate in regions of low shear rate. Figure 3 shows that the migration in our experiments scales with the bulk concentration, n_0L^2d: comparing on the basis of volume fraction would result in similar values for the extent of migration at volume fractions different by factors of approximately 2, the ratio of the aspect ratios studied here. This differs with the conclusion from measurements in Couette flows [18] that fiber migration scales with volume fraction irrespective of the aspect ratio, though those experiments used a narrower and higher concentration range of $\phi = 0.3$–0.4 than used here ($\phi = 0.03$–0.21). Predictions [19] using a continuum model relying on constitutive laws [6,25] show that migration depends only upon the volume fraction in Couette flows, but depends on the aspect ratio at the same volume fraction in parabolic flows. Stokesian dynamics simulations of spherical doublets in a pressure-driven flow predicted migration similar to that of spheres, when compared at the same bulk volume fractions [20], but the aspect ratio was much lower than those examined here.

The measured extent of migration is maximum at $n_0L^2d = 0.84$, as shown in Fig. 3(b). As n_0L^2d surpasses 1, the extent of migration likely becomes increasingly hindered by the difficulty

of packing additional particles in the central region of the pipe. A similar phenomenon occurs for shear-induced migration of spheres, where concentrations observed at the center of the pipe do not exceed maximum random packing. For rigid fibers, a similar constraint would be a severe one, since the maximum random packing scales as $1/A$ for large aspect ratios [26]. In our experiments, the maximum number density measured at the center of the pipe was $n(r/R = 0) = 4/L^2 d$ [see Fig. 2(b)], or equivalently $\phi(r/R = 0) = 0.29$. This falls below an estimate of $\phi \approx 0.4$ [27] at which a collection of spherocylinders with $A = 11$ can remain randomly oriented. Still, bundles of rigid fibers having highly correlated alignments can be seen in the experimental images (see image in Fig. 2(b) and Movie 3 [24]). The occurrence of oriented crystallites suggests that the migration and shearing flow may be promoting a transition toward a nematic phase. Moreover, this phase transition would enable concentrations beyond the limit of maximum random packing.

Migration of spherical particles in parabolic flows has been reported for volume fractions as low as 20%, but not at 10% [22]. Data shown here indicate that migration can occur in suspensions of fibers at volume fractions as low as $\phi \approx 0.03$. This includes results for $n_0 L^2 d = 0.84$ and $A = 23$, as indicated in Fig. 3(b) and its inset where the concentration profile is shown. Migration might occur for spheres at volume fractions of 10%, or even less, but the total strain required for spheres to attain a steady profile increases drastically as the concentration drops and also depends strongly on the ratio of particle size to pipe size. Similarly, Fig. 3(a) demonstrates that rigid fibers require a larger total strain at smaller values of $n_0 L^2 d$ to attain a steady concentration profile. The rate of migration was similar for the two batches of fibers having identical lengths, but diameters different by a factor of about 2.

For dilute conditions, fibers rotating lengthwise in shearing flows can contact the bounding walls, generating an irreversible force and associated depletion layer of thickness $\approx L/2$ [28]. For the ratio of R/L studied here, this "pole-vault" motion would cause a deficit of particles for $r/R > 0.68$, and there would be no significant concentration gradient for $r/R < 0.68$ in the absence of a shear-induced migration. For concentrations beyond dilute, the pole-vault motion might still lead to a depletion region even though the motion becomes hindered by contacts with other fibers. No evidence of a clear depletion layer is seen in the concentration data, nor any of the visualizations (see movies [24]). Even in the most dilute case of $n_0 L^2 d = 0.42$ and $A = 11$, where a depletion layer would be most evident, there is no significant migration relative to the measured fluctuations in the mean concentrations as seen in the inset of Fig. 3(b).

Measurements of the orientation distributions (see Fig. 4) are largely consistent with expectations of fiber alignment with the flow, rather than the gradient, direction in steady shearing flows. The confinement of the rigid fibers is notably impacting the orientations near the wall: the probability distribution of ψ' shifts strongly toward flow alignment as the radial position moves near the wall. Likewise, there is a shift toward vorticity alignment as the radial position moves toward the wall, as seen by comparing the results for $2R/3 < r < R$ with the other two regions as seen in Fig. 4(b). However, confinement is strong in these experiments and it is assumed to affect orientation in simple shear flows. The enhanced vorticity alignment for fibers near the bounding walls of the pipe is indeed reminiscent of the vorticity alignment observed in oscillatory shear flows [5,29] for highly confined suspensions. A tendency to align in the vorticity direction has not been reported for steady shearing flows of rigid fibers [3,4]; consequently it may be that the oscillations in the pipe flow are driving the vorticity alignment.

Likewise, the oscillations may be impacting the spatial distribution of the particles. Experiments utilizing strain amplitudes less than 15 exhibited less migration at the same concentration, accumulated strain, and aspect ratio. This difference in results can be attributed to the rearrangement of the microstructure with the flow upon shear reversal, a problem which also occurs in the oscillatory study of spheres [22]. Note that the strain required for a fiber of aspect ratio of 11 to complete a full Jeffrey orbit [30], as evaluated at the mean rate of shear in the pipe flow, exceeds the strain amplitude used in the experiments reported here by about 30%. However, a strain equivalent to that required for a full Jeffrey orbit is not necessarily required for the microstructure to reach steady state at high concentrations. Experiments with a strain amplitude larger than 15 were not conducted for

the fibers due to the limitation imposed by the total length of the pipe; the extent of migration may increase as the strain amplitude is increased.

In conclusion, the present work demonstrates that, as observed with spheres, fibers migrate toward the center of the pipe in parabolic flows. Our measurements suggest that $\phi_0 A$ ($\propto n_0 L^2 d$), rather than simply the volume fraction ϕ_0, controls the extent of migration, and the migration is seen to be maximized at $n_0 L^2 d \approx 1$. An important output is that the fiber orientation varies spatially, with the orientation of the fibers in the near-wall region aligning more strongly in the flow direction than at the center. However, there is also an enhanced probability of fibers near the wall aligning in the vorticity direction. Additional experiments or simulations are needed to explore the role of the confinement in the extent of migration and orientation distribution, and to confirm whether or not the oscillatory experiments presented here produce the same migration as a steady pipe flow.

This work has been carried out thanks to the support of the ANR project "Dense Particulate Systems" (ANR-13-IS09-0005-01), the "Laboratoire d'Excellence Mécanique et Complexité" (ANR-11-LABX-0092), the Excellence Initiative of Aix-Marseille University–A*MIDEX (ANR-11-IDEX-0001-02) funded by the French Government "Investissements d'Avenir programme," and COST Action MP1305 "Flowing Matter." S. Shaikh benefited from a fellowship of the A*MIDEX Excellence Academy–Ph.D. Collegium. This work was also supported by the National Science Foundation (Grants No. 1511787 and No. 1362060).

[1] J. E. Butler and B. Snook, Microstructural dynamics and rheology of suspensions of rigid fibers, Annu. Rev. Fluid Mech. **50**, 299 (2018).

[2] M. Hassanpoura, P. Shafighb, and H. B. Mahmudb, Lightweight aggregate concrete fiber reinforcement—A review, Constr. Build. Mater. **37**, 452 (2012).

[3] C. A. Stover, D. L. Koch, and C. Cohen, Observations of fibre orientation in simple shear flow of semi-dilute suspensions, J. Fluid Mech. **238**, 277 (1992).

[4] M. P. Petrich, M. Chaouche, D. L. Koch, and C. Cohen, Oscillatory shear alignment of a non-Brownian fiber in a weakly elastic fluid, J. Non-Newtonian Fluid Mech. **91**, 1 (2000).

[5] A. Franceschini, E. Filippidi, E. Guazzelli, and D. J. Pine, Transverse Alignment of Fibers in a Periodically Sheared Suspension: An Absorbing Phase Transition with a Slowly Varying Control Parameter, Phys. Rev. Lett. **107**, 250603 (2011).

[6] D. Leighton and A. Acrivos, The shear-induced migration of particles in concentrated suspensions, J. Fluid Mech. **181**, 415 (1987).

[7] J. R. Abbott, N. Tetlow, A. L. Graham, S. A. Altobelli, E. Fukushima, L. A. Mondy, and T. S. Stephens, Experimental observations of particle migration in concentrated suspensions: Couette flow, J. Rheol. **35**, 773 (1991).

[8] S. A. Altobelli, R. C. Givler, and E. Fukushima, Velocity and concentration measurements of suspensions by nuclear magnetic resonance imaging, J. Rheol. **35**, 721 (1991).

[9] S. W. Sinton and A. W. Chow, NMR flow imaging of fluids and solid suspensions in Poiseuille flow, J. Rheol. **35**, 735 (1991).

[10] C. J. Koh, P. Hookham, and L. G. Leal, An experimental investigation of concentrated suspension flows in a rectangular channel, J. Fluid Mech. **266**, 1 (1994).

[11] N. Phan-Thien, A. L. Graham, S. A. Altobelli, J. R. Abbott, and L. A. Mondy, Hydrodynamic particle migration in a concentrated suspension undergoing flow between rotating eccentric cylinders, Ind. Eng. Chem. Res. **34**, 3187 (1995).

[12] R. E. Hampton, A. A. Mammoli, A. L. Graham, N. Tetlow, and S. A. Altobelli, Migration of particles undergoing pressure-driven flow in a circular conduit, J. Rheol. **41**, 621 (1997).

[13] M. K. Lyon and L. G. Leal, An experimental study of the motion of concentrated suspensions in two-dimensional channel flow. Part 1: Monodisperse systems, J. Fluid Mech. **363**, 25 (1998).

[14] N. Tetlow, A. L. Graham, M. S. Ingber, S. R. Subia, L. A. Mondy, and S. A. Altobelli, Particle migration in a Couette apparatus: Experiment and modeling, J. Rheol. **42**, 307 (1998).
[15] P. R. Nott and J. F. Brady, Pressure-driven flow of suspensions: Simulation and theory, J. Fluid Mech. **275**, 157 (1994).
[16] P. R. Nott, E. Guazzelli, and O. Pouliquen, The suspension balance model revisited, Phys. Fluids **23**, 043304 (2011).
[17] B. Snook, L. M. Davidson, J. E. Butler, O. Pouliquen, and E. Guazzelli, Normal stress differences in suspensions of rigid fibres, J. Fluid Mech. **758**, 486 (2014).
[18] L. A. Mondy, H. Brenner, S. A. Altobelli, J. R. Abbott, and A. L. Graham, Shear-induced particle migration in suspensions of rods, J. Rheol. **38**, 444 (1994).
[19] X. Fan, N. Phan-Thien, and R. Zheng, Simulation of fibre suspension flow with shear-induced migration, J. Non-Newtonian Fluid Mech. **90**, 47 (2000).
[20] A. Singh, Dynamics of suspensions of spherical doublets in simple shear and pressure driven flow, Chem. Eng. Sci. **104**, 17 (2013).
[21] J. E. Butler, P. D. Majors, and R. T. Bonnecaze, Shear-induced particle migration for oscillatory flow of a suspension within a tube, Phys. Fluids **11**, 2865 (1999).
[22] B. Snook, J. E. Butler, and É. Guazzelli, Dynamics of shear-induced migration of spherical particles in oscillatory pipe flow, J. Fluid Mech. **786**, 128 (2016).
[23] O. L. Forgacs and S. G. Mason, Particle motions in sheared suspensions: IX. Spin and deformation of threadlike particles, J. Colloid Sci. **14**, 457 (1959).
[24] See Supplemental Material at http://link.aps.org/supplemental/10.1103/PhysRevFluids.3.091301 for Movies 1–3 showing experiments for bulk concentrations of 0.84, 1.68, and 3.00, respectively, and Movies 4 and 5 showing processed data and results for bulk concentrations of 0.84 and 3.00.
[25] R. J. Phillips, R. C. Armstrong, R. A. Brown, A. L. Graham, and J. R. Abbott, A constitutive equation for concentrated suspensions that accounts for shear-induced particle migration, Phys. Fluids A **4**, 30 (1992).
[26] M. Nardin, E. Papirer, and J. Schultz, Contribution a l'étude des empilements au hasard de fibres et/ou de particules sphériques, Powder Technol. **44**, 131 (1985).
[27] S. R. Williams and A. P. Philipse, Random packings of spheres and spherocylinders simulated by mechanical contraction, Phys. Rev. E **67**, 051301 (2003).
[28] Carl A. Stover and C. Cohen, The motion of rodlike particles in the pressure-driven flow between two flat plates, Rheol. Acta **29**, 192 (1990).
[29] B. Snook, É. Guazzelli, and J. E. Butler, Vorticity alignment of rigid fibers in an oscillatory shear flow: Role of confinement, Phys. Fluids **24**, 121702 (2012).
[30] G. B. Jeffery, The motion of ellipsoidal particles immersed in a viscous fluid, Proc. R. Soc. London A **102**, 161 (1922).